2016

Development Of Core Ion Temperature Gradients And Edge Sheared Flows In A Helicon Plasma Device Investigated By Laser Induced Fluorescence Measurements

S. C. Thakur

J. J. Gosselin

J. McKee

E. E. Scime

S. H. Sears

See next page for additional authors

Development of core ion temperature gradients and edge sheared flows in a helicon plasma device investigated by laser induced fluorescence measurements

S. C. Thakur,[1,2] J. J. Gosselin,[2] J. McKee,[3] E. E. Scime,[3] S. H. Sears,[3,a)] and G. R. Tynan[1,2]
[1]*Center for Momentum Transport and Flow Organization, University of California at San Diego, San Diego, California 92093, USA*
[2]*Center for Energy Research, University of California at San Diego, San Diego, California 92093, USA*
[3]*Department of Physics and Astronomy, West Virginia University, Morgantown, West Virginia 26506, USA*

(Received 17 May 2016; accepted 27 July 2016; published online 15 August 2016)

We report experimental observation of ion heating and subsequent development of a prominent ion temperature gradient in the core of a linear magnetized plasma device, and the controlled shear de-correlation experiment. Simultaneously, we also observe the development of strong sheared flows at the edge of the device. Both the ion temperature and the azimuthal velocity profiles are quite flat at low magnetic fields. As the magnetic field is increased, the core ion temperature increases, producing centrally peaked ion temperature profiles and therefore strong radial gradients in the ion temperature. Similarly, we observe the development of large azimuthal flows at the edge, with increasing magnetic field, leading to strong radially sheared plasma flows. The ion velocities and temperatures are derived from laser induced fluorescence measurements of Doppler resolved velocity distribution functions of argon ions. These features are consistent with the previous observations of simultaneously existing radially separated multiple plasma instabilities that exhibit complex plasma dynamics in a very simple plasma system. The ion temperature gradients in the core and the radially sheared azimuthal velocities at the edge point to mechanisms that can drive the multiple plasma instabilities, that were reported earlier. *Published by AIP Publishing.*
[http://dx.doi.org/10.1063/1.4960824]

I. INTRODUCTION

Studies of gradient driven turbulence are crucial to plasma physics, as the loss of particles and energy from the confinement regions of magnetically confined fusion plasma is believed to be driven by turbulent drift wave fluctuations associated with the cross-field gradients in density and temperature.[1,2] Drift waves can also non-linearly drive poloidally and toroidally symmetric large scale sheared $\mathbf{E} \times \mathbf{B}$ plasma flows, called zonal flows, via the turbulent Reynolds Stress.[3] The interactions between drift wave turbulence and zonal flows are crucial in understanding the saturation mechanisms of turbulence, thus leading to improved confinement in fusion devices. Hence, drift wave turbulence—zonal flow physics research has been actively pursued by several research groups related to magnetized plasmas and controlled fusion. Linear magnetized devices allow the detailed study of zonal flow and drift wave turbulence due to their simpler geometry and better access for diagnostics.[4–10] In addition, in fusion devices, instabilities associated with temperature gradients (both the ion and the electron temperatures) can play an important role establishing various regimes of operation.[11,12] Existence of strong shear flows can also give rise to various kinds of velocity shear driven instabilities[13] in addition to the classical Kelvin-Helmholtz instability. Ion temperature measurements are important not only to measure existing temperature gradients but also to calculate the relevant damping terms, such as the ion-ion viscosity, for the drift waves. Hence, in these experiments, we measure the radial profiles of the relevant plasma quantities like the ion temperature and the azimuthal plasma velocity to help in understanding the various energy sources that drive different instabilities.

Previous studies in the Controlled Shear Decorrelation eXperiment (CSDX)[4–6] had demonstrated controlled transition to drift wave turbulence as the magnetic field ($\mathbf{B}$) is increased from 400 G to 1000 G when the device is configured with insulating end plate boundary conditions.[14,15] With increasing $\mathbf{B}$, the density gradient driven resistive drift wave fluctuations evolve from narrow-band coherent fluctuations to a state of weak turbulence characterized by broadened frequency and wave number spectra. At $\mathbf{B} = 1000$ G, coherent mode-like drift wave fluctuations (with a dominant $m = 3$ mode) coexist with a broadband background of turbulent fluctuations. For $\mathbf{B} > 800$ G, studies in CSDX also show the presence of a turbulence driven azimuthally symmetric shear flow without any external sources of momentum input, such as biasing.[4,5] Nonlinear energy transfer analyses[6,16] have shown that for $\mathbf{B} = 1000$ G, the energy is transferred from relatively higher frequency ($f > 10$ kHz) turbulent fluctuations to low frequency ($f < 1$ kHz) azimuthally symmetric shear flow, thus showing the characteristics of a zonal flow.

More recent experiments on the upgraded CSDX,[7] which uses a larger diameter (15 cm) source and m = 1 helical RF antenna, have shown that, when the magnetic field is increased even further, a global change in the system occurs

[a)]Currently at the University of Wisconsin at Madison, Madison, Wisconsin 53706, USA.

at a threshold magnetic field ($\mathbf{B_{th}}$ which depends on the source parameters). Below $\mathbf{B_{th}}$, the plasma is dominated by density gradient driven collisional drift wave instabilities, with the modes propagating in the electron diamagnetic drift direction. For $\mathbf{B} > \mathbf{B_{th}}$, a new global equilibrium is achieved with the simultaneous existence of three radially separated plasma instabilities: coherent high azimuthal mode number fluctuations in the central core; collisional drift waves in the density gradient region; and strong, turbulent, shear-driven instabilities at the edge. The coherent high azimuthal modes at the center propagate in the ion diamagnetic drift direction, while in the other regions the fluctuations propagate in the electron diamagnetic drift direction. This was directly observed using fast framing imaging[17] and with multi point Langmuir probe measurements.[18] The radial particle flux is directed outward for small radii and inward for large radii, thus forming a radial particle transport barrier which leads to stiff profiles and increased core plasma density.[7,18,19] Simultaneously, the Ar-II light emission from the central region increases by an order of magnitude leading to the formation of a very bright blue core. The radial extent of the inner coherent modes and radial location of the particle transport barrier define the radial extent of the inner blue core.[7,19] This new global equilibrium with the three simultaneously present radially separated plasma instabilities shows very rich plasma dynamics including intermittency, formation and propagation of blobs, formation of a radial transport barrier, inward particle flux[18] against density gradients, etc. More recent observation points to a transport bifurcation phenomenon behind the physics of this transition.[20] Several plasma phenomena are observed during this global transition in the upgraded CSDX, and more work is being undertaken to understand the details. To identify the various instability mechanisms and explain the features, we are pursuing more detailed measurements of relevant plasma parameters such as the ion temperature profiles and the Doppler resolved absolute ion fluid velocity profiles.

Laser Induced Fluorescence (LIF) is a standard spectroscopic diagnostics used in helicon[21] plasma sources to measure the Doppler resolved velocity distribution functions (VDF) of various species such as argon ions, argon neutrals, helium neutrals, and xenon ions.[22–24] The full width at half maxima (FWHM) of the VDF is a measure of the average temperature of the distribution. The shift of the peak of the VDF from a standard reference line gives the absolute ion fluid velocity. If the ion diamagnetic drift velocity is computed from the density and the ion temperature profiles, then the $\mathbf{E} \times \mathbf{B}$ drift profile is also found. In this paper, we show argon ion LIF measurements of the radial profiles of the azimuthal velocity and the ion temperature of the upgraded CSDX plasma in conditions that range from stable collisional drift wave dominated regimes to the state after the global transition where we observe the three simultaneously existing, radially separated plasma instabilities. These measurements confirm the presence of strongly sheared ion fluid flows at the edge of the plasma, consistent with observations of high intensity shear driven fluctuations in the edge region.[7,17] The observed ion heating at the central plasma core, near the global transition threshold, points to an instability mechanism (ion temperature gradient driven instabilities) that explains several features of the coherent modes observed at the center of the plasma.

II. EXPERIMENTAL APPARATUS

The experiments were carried out in the upgraded version of the Controlled Shear De-correlation eXperiment (CSDX), a cylindrical magnetized helicon plasma device.[7] The plasma is contained in a stainless steel vacuum chamber, 2.8 m long with a diameter of 0.20 m, as shown in Fig. 1(a). The argon plasma is produced by a 13.56 MHz, 1.5 kW (can go to a maximum RF power of 5.5 kW), $m = 1$ helicon antenna having a diameter of 0.15 m, wrapped around a bell jar at one end of the vacuum chamber. The reflected power is kept less than 20 W, and the chamber and the source are immersed in an axially uniform magnetic field of strength up to 2400 G. These experiments were performed at a neutral gas fill pressure of 3.2 mTorr. More details of the experimental device, the operating regimes, and the standard plasma diagnostics used on CSDX can be found elsewhere.[7,25] At the standard operating conditions, typical electron temperatures and plasma densities in CSDX, as measured by RF compensated, cylindrical Langmuir probes are $T_e \sim 3$–4 eV and $n \sim 10^{13}\,\mathrm{cm}^{-3}$, respectively. In Fig. 2, we show an example of the typical radial profiles of the density, electron

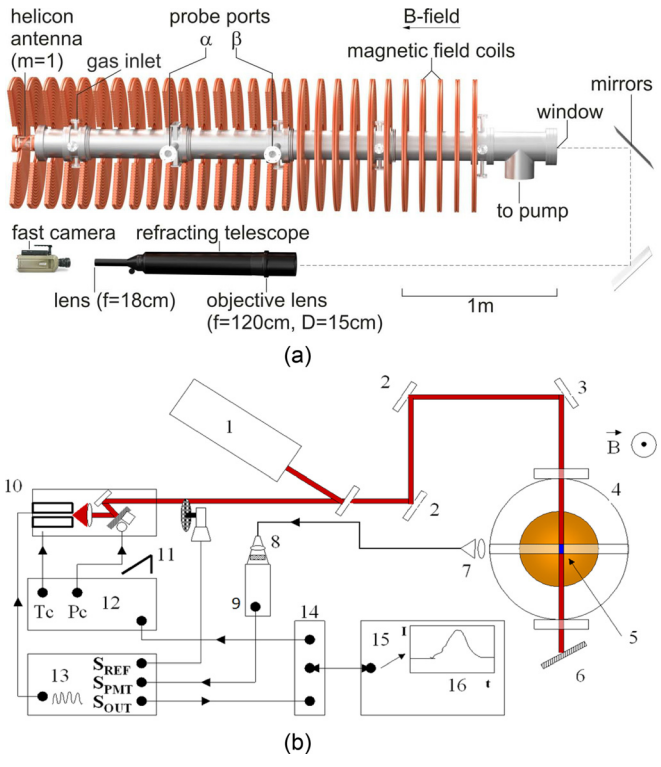

FIG. 1. (a) Schematic of CSDX. The laser light is injected from the top at the port location named α, and the fluorescent emission is collected at the same location from the side; and (b) LIF set up where 1—wavemeter, 2—laser beam steering optics, 3—laser beam injection mirror, 4—cross section of plasma chamber, 5—LIF volume of interrogation, 6—laser beam dump, 7—collection optics (collimator and optical fiber), 8—interference filter for 443 nm, 9—photo-multiplier tube (PMT), 10—Toptica tapered amplified laser, 11—mechanical chopper, 12—laser controller module, 13—lock-in amplifier, 14—data acquisition card, 15—laptop PC, and 16—LIF signal (intensity vs. wavelength) for real time monitoring.

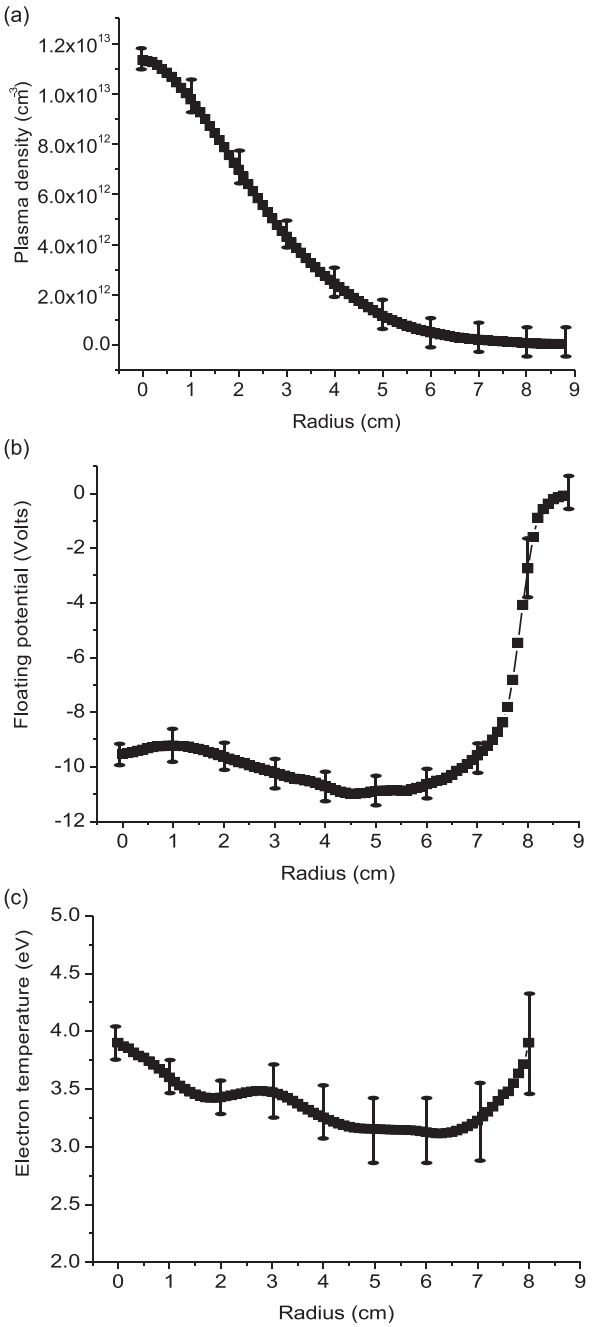

FIG. 2. Radial profiles of (a) plasma density, (b) floating potential, and (c) electron temperature, measured for $\mathbf{B} = 1000$ G.

temperature, and the floating potentials measured at $\mathbf{B} = 1000$ G. Full sets of radial profiles of the plasma density, electron temperature, and floating potential as the magnetic field is scanned from low ($\mathbf{B} = 400$ G) to high ($\mathbf{B} = 2400$ G) fields are shown in Figs. 2–4 of Ref. 7. In this paper, we primarily focus on the results from LIF measurements in the magnetic field range from 400 G to 1800 G, as the $\mathbf{B_{th}} \sim 1300$ G, and we have seen that after the transition the plasma parameters do not undergo any major changes.[7,19] We had also previously found that the end boundary conditions can play a crucial role in suppressing or enhancing the level of turbulence in CSDX.[14,15] To be consistent with the previous experiments,[7] the insulating boundary conditions are used here too. All other external parameters for the helicon source, such as the neutral gas pressure, the gas flow rate, and the forward and reflected powers, were kept constant throughout these experiments.

The LIF measurements shown here were obtained via crossed beam injection and collection, as shown in Fig. 1(b), similar to the configuration used in a previous campaign of LIF experiment on the original CSDX with an $m = 0$ antenna, smaller source diameter (10 cm), and reduced magnetic fields.[26,27] The laser light was injected perpendicular to the background magnetic field using a rectangular glass window at the top of the plasma vacuum chamber, located 75 cm downstream from the helicon antenna. The argon ions are Doppler shifted along the path of the injected light, and hence this yields the perpendicular ion temperature and the azimuthal ion fluid velocities. We used optics mounted on a manually controlled linear stage to inject the laser light at different radial locations, thus enabling us to obtain radial profiles of the azimuthal ion velocities and perpendicular ion temperatures. The induced fluorescence light emission was collected through one of the side ports of the chamber at the same axial location as the injected beam. The collection lenses were placed on another manually controlled linear stage which was adjusted in tandem with the radial location of the laser injection optics. This ensured that the interrogated plasma volume (the cross over between the beam lines of the injected laser light and the volume which was seen by the collection optics) and hence the solid angle of the fluorescence emission remained constant for each radial measurement.

For LIF measurements, a Toptica TA 100 tunable diode laser was used. The laser consisted of a master oscillator diode in a Littrow configuration followed by a tapered amplifier. The laser, with a line width of <1 MHz, had a mode hop free tuning range of $\sim$30 GHz. Tuning was critical, and a small diode current feedback loop was used to achieve the maximum possible stable tuning range. To measure the argon ion velocity distribution function (IVDF), the laser was scanned around the central absorption line at 668.6138 nm, corresponding to $3d^4\ F_{7/2}$ to $4p^4\ D_{5/2}$ level transition in Ar II.[28] To prevent stray reflections from damaging the diode laser, high attenuation optical isolators were inserted between the master oscillator and the amplifier and also between the amplifier and the first optical component outside the laser housing. An 8% sampling beam-splitter and lens system was used to direct the sampled light into a fiber optic coupled Bristol Instruments 621-VIS wavemeter for real time wavelength monitoring, with an instrumental accuracy of ± 0.00005 nm. The central laser wavelength was also verified by comparing to NIST published database of iodine emission spectroscopy using an iodine cell.[28] The error in the measured azimuthal velocity due to this instrumental error is approximately ± 25 m/s. The laser is scanned across about 10–14 GHz, with a wavelength resolution of 5 data points per GHz to measure each IVDF. The other 92% of the laser light was mechanically chopped at a few kHz for use with a lock-in-amplifier for phase synchronous detection and transported to the plasma chamber by beam steering mirrors.

The fluorescent emission signal at 442.60 nm from the decay of $4p^4D_{5/2}$ state to the $4s^4P_{3/2}$ state was coupled into an optical fiber using a 2 in. optical lens and collimator. The

light exiting from the fiber was re-collimated into a visible light Hamamatsu photo-multiplier tube (PMT). We used a 1 nm wide filter centered at 443 nm to prevent unwarranted Ar II light from the background plasma from entering the PMT. The intensity of the fluorescent emission due to the excitation by the laser, as a function of the scanned laser frequency, is a direct measurement of the IVDF in the spatial region where the injected laser beam path overlaps the collection volume. In this experiment, the spatial resolution of the LIF measurements was ~3 mm. Since the PMT signal was composed of background spectral radiation, electron-impact-induced fluorescence radiation, and electronic noise (taken together they are an order of magnitude larger than the actual laser induced fluorescence signal), a Stanford Research SR830 lock-in amplifier, synchronized to the mechanical chopper, was used for phase synchronous detection of the LIF signal.

In the presence of a finite magnetic field, the 668.6138 nm Ar II transition line undergoes Zeeman splitting consisting of 12 circularly polarized sigma (σ: $m = \pm 1$) and 6 linearly polarized pi (π: $m = 0$) transitions.[29] It has been shown that for similar helicon plasmas, the Zeeman effect and the thermal broadening are the only two line broadening mechanisms that define the IVDF, and all other line broadening mechanisms are negligibly small.[30] The Zeeman σ lines are split symmetrically into two clusters of lines corresponding to the $m = \pm 1$ components, and they are the biggest contributors to the Zeeman broadening of the IVDF. The Zeeman broadening happens when each individually Zeeman split cannot be resolved spectroscopically and the IVDF seems artificially broadened. As shown in Fig. 3, for $\mathbf{B} = 1000$ G, after proper weighing of the split lines by their intensity, the average extent of the spread of the σ lines is $\sim 4.44 \times 10^{-3}$ nm, which at 668.6138 nm gives a spectral width of ~2.98 GHz. However, for the same $\mathbf{B} = 1000$ G, the π lines have on an average, a line weighted spread of $\sim 9.8 \times 10^{-4}$ nm, which at 668.6138 nm yields only a spectral width of ~0.66 GHz. For typical ion temperatures of CSDX, the injected laser frequency scan necessary for capturing a complete IVDF typically spanned ~12 GHz. Thus, the effect of Zeeman splitting of the π lines is quite small for the magnetic field strengths considered in this experiment. The

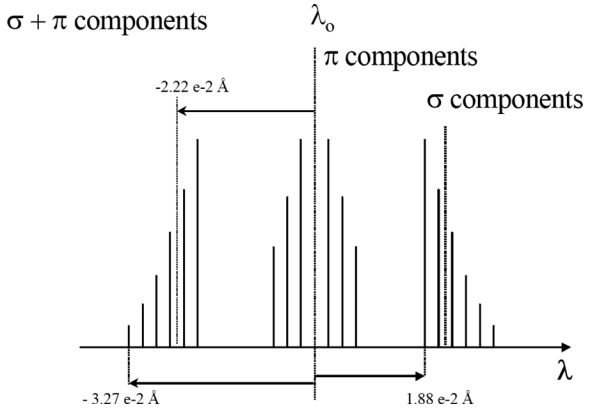

FIG. 3. Zeeman splitting of the 668.8138 nm Ar II line, showing the spectral spread of the 12 circularly polarized sigma (σ: $m = \pm 1$) and 6 linearly polarized pi (π: $m = 0$) transitions. The calculations are done for B = 1000 G.

typical IVDF full width at half maximum, which is proportional to the ion temperature, is ~4–6 GHz for these plasmas (see Fig. 4). To ensure that only the π absorption lines are excited, the laser is injected perpendicular to the magnetic field with its polarization axis aligned with the magnetic field (once the perpendicular injection is decided, one can rotate the axis of polarization of the laser until it is ensured that the axis is parallel to the magnetic field, thus being linearly polarized). This choice of the polarization of the injected laser light preferentially selects only the π lines and reduces the effects of Zeeman splitting. Even for the largest magnetic field strength used in this study ($\mathbf{B} = 1800$ G), the effect of Zeeman splitting of only the π lines is much smaller than that due to Doppler broadening and thus is ignorable in the analysis. A single Gaussian fit gives results as good as a deconvoluted fit, within the standard statistical errors from the experiment. For example, at the maximum magnetic field of this experiment (1800 G), we found that the difference between using the full Zeeman deconvolution signal analysis (to account for Zeeman splitting)[29] and a simple single Gaussian fit is only 0.04 eV, which is typically smaller than the statistical errors from the standard deviations of multiple measurements of ion temperatures.

III. RESULTS

The measured IVDF is used to calculate the Doppler broadened temperature and the Doppler shifted velocity. The full width at half maxima (FWHM) of the IVDF is proportional to the average perpendicular argon ion temperature, while the shift of the peak of the VDF from a standard reference line (we used an iodine cell to check the center of the distribution corresponding to zero velocity)[31] gives the absolute ion fluid velocity, in the azimuthal direction. A nonlinear least square fitting routine is used to fit the measured IVDF with a single drifting Maxwellian distribution of the form

$$I_R(v) = I_R(v_0) \cdot \exp \cdot [-m_{ion} \cdot c^2 \cdot (v - v_0)^2 / (2k_B \cdot T_{ion} \cdot v_0^2)], \quad (1)$$

where $I_R(v)$ is the intensity of the fluorescence signal at any given frequency v, v_o is the rest frame frequency of the absorption line, m_{ion} is the ion mass, c is the speed of light, k_B is the Boltzmann constant, and T_{ion} is the ion temperature. For using in the fitting routine, Eq. (1) reduces to

$$I_R(v) = I_R(v_o) \cdot \exp \cdot [-(v - v_o)^2 / (\alpha_D T_{ion})], \quad (2)$$

where α_D is the Doppler fitting parameter. When the scanning frequency is measured in GHz and the ion temperature in eV, this Doppler fitting parameter calculated for the 668.6138 transition is: $(\alpha_D)^{-1} = 0.092494$ eV $(\text{GHz})^{-2}$.

In Fig. 4, we show and compare examples of the measured IVDF for both $\mathbf{B} = 1400$ G [Figs. 4(a) and 4(c)] and $\mathbf{B} = 400$ G [Figs. 4(b) and 4(d)], at $r = 0$ cm [Figs. 4(a) and 4(b)] and at $r = 3$ cm [Figs. 4(c) and 4(d)]. Each measured IVDF is fit to Equation (2) to obtain the fit Doppler broadened perpendicular ion temperature and the Doppler shifted absolute ion fluid velocity. Embedded in Fig. 4 are the fit

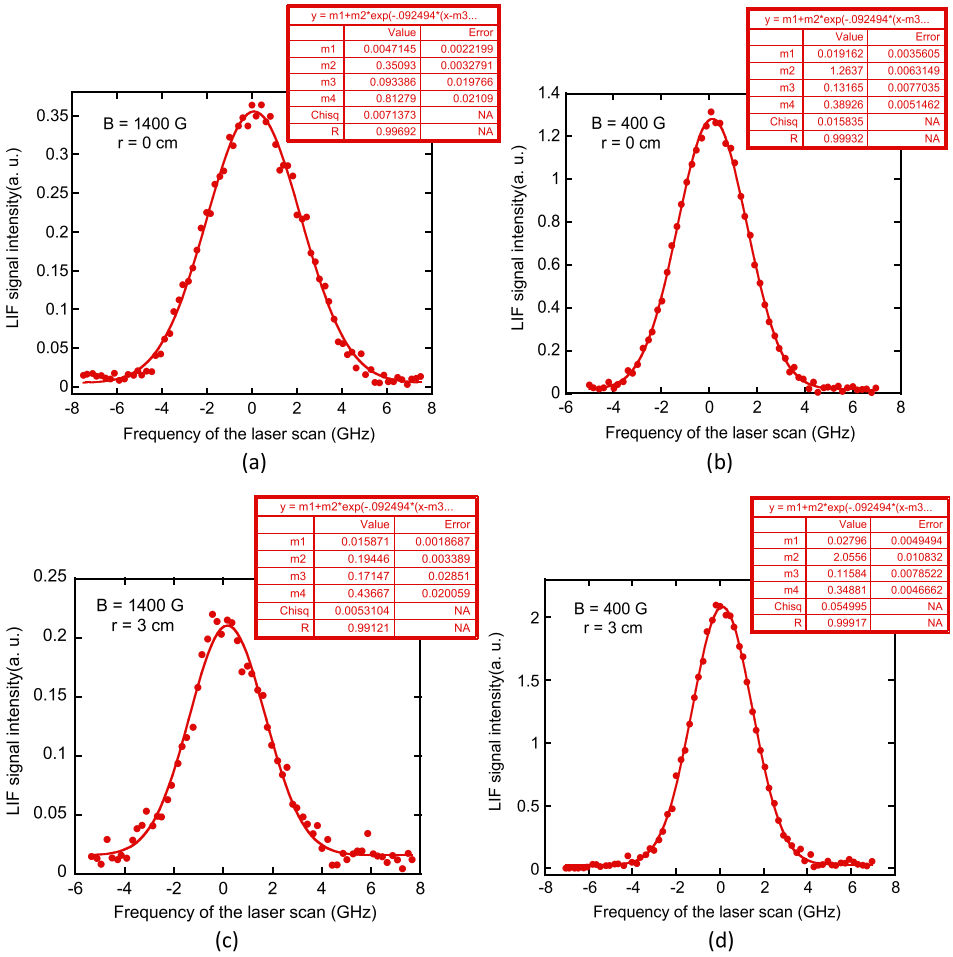

FIG. 4. Examples of some measured IVDFs from LIF and the corresponding fits, shown for two magnetic fields, $\mathbf{B} = 1400$ G and $\mathbf{B} = 400$ G, at for two radial locations, r = 0 and r = 3. The formula used for fitting the collected light intensity (y) as a function of frequency (x) is given by $\boldsymbol{y = m1 + m2 \times \exp.\,[-0.92494 \times (x - m3)^2/m4]}$, where the parameter **m3** gives the absolute Doppler shifted ion fluid velocity in GHz, and the parameter **m4** gives the ion temperature in eV. Note that the scatter in the measured IVDF is larger for turbulent plasma [$\mathbf{B} = 1400$ G; (a) and (c)] even with more averaging than that in the more coherent and quiescent plasma [$\mathbf{B} = 400$ G; (b) and (d)].

parameters generated out of the non-linear fitting routine. We clearly see the change in the ion temperature from the FWHM of the IVDFs at different magnetic fields and various radii. The scatter shown in the plots is mainly due to the fluctuations in the emitted light intensity, which are proportional to plasma density fluctuations within the experimentally probed volume of plasma. We find that for plasma conditions dominated by coherent drift waves (at relatively low **B**), the scatter in the plots is minimal, as shown for the case of $\mathbf{B} = 400$ G in Figs. 3(b) and 3(d). The density fluctuations are more coherent, and their contribution to the total signal is minimized by averaging over the timescale of the measurement (for each wavelength step during the scan, 200–500 points were averaged using the lock-in amplifier to create each data point in the plot). At increased magnetic fields, the fluctuations are not strictly periodic (consisting of multiple modes leading to turbulence), and they persist even after averages over 1000 measurements are performed. The strong deviation from the best fit is not just simply electronic noise, but real fluctuations in the emitted LIF signal due to turbulent density perturbation within the plasma volume of interrogation, as seen for $\mathbf{B} = 1400$ G in Figs. 4(a) and 3(c). To obtain acceptable signal-to-noise levels in the measured IVDFs, multiple such scans (with 30 s integration time for each laser frequency step) are recorded and then averaged together. For strongly turbulent plasmas at large radii, recording several scans and averaging them together still did not reduce the scatter significantly in the measured IVDF, but the ensemble of points from all the scans is reasonably well fit by a single Gaussian. Moreover, since at large radii, the density also goes down by almost one order of magnitude,[7] the actual LIF signal decreases in strength, and the signal to noise ratio also decreased. The scatter in the plots provides a rough estimate of the plasma density fluctuation profile at different radial locations and for different parameters.

Figs. 5(a) and 5(b) show the radial profiles of the perpendicular ion temperature as the magnetic field is increased, starting from relatively low magnetic fields ($\mathbf{B} = 400$ G), where the plasma is still dominated by coherent resistive drift wave modes.[5–7] As **B** is gradually increased to 1000 G, the spectral features start broadening, thus signifying a controlled transition to resistive drift wave turbulence. The global transition[7,19] in the upgraded CSDX happens between 1300 G and 1400 G, where multiple instabilities are simultaneously present in the system and the spectral features are very broad (though it is noted that the intensity of the turbulence features drop after this global transition). Hence, for clarity, we divide the magnetic field scan into two parts: 400 G–1000 G, which represents the controlled transition to drift wave turbulence driven by the density gradient (but is still far away from the global transition, in the magnetic field parameter space) and then from 1100 G to 1400 G, to understand the details near the transition to the global transition at $\mathbf{B} \sim 1300$ G. Typical errors in these measurements, calculated from statistical deviation from multiple measurements, are $\sim \pm 0.02$ eV for $r < 3$ cm and $\sim \pm 0.04$ eV for $r > 4$ cm. For

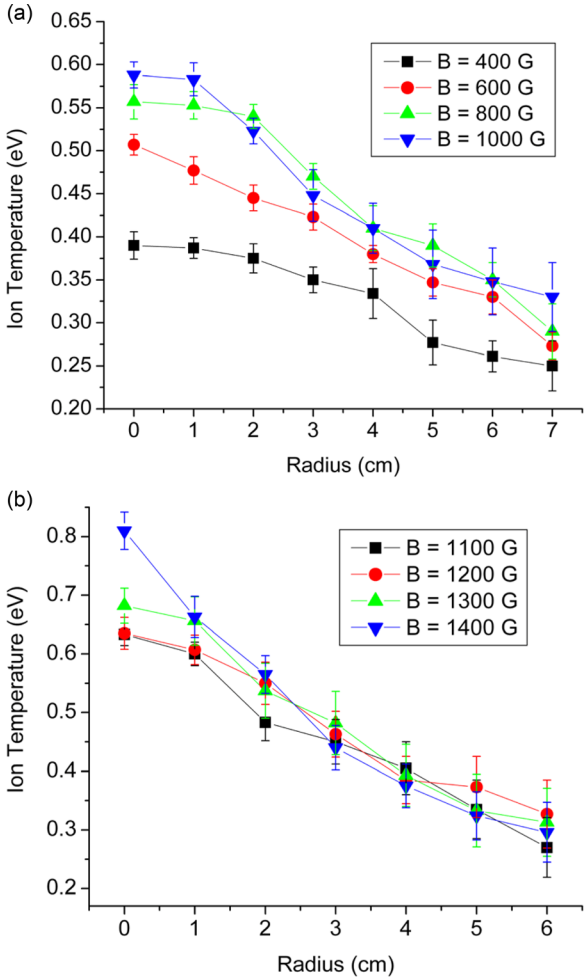

FIG. 5. (a) Radial profiles of the perpendicular ion temperature at 400 G (black squares), 600 G (red circles), 800 G (green upright triangles), and 1000 G (blue inverted triangles). (b) Radial profiles of the perpendicular ion temperature at 1100 G (black squares), 1200 G (red circles), 1300 G (green upright triangles), and 1400 G (blue inverted triangles).

$\mathbf{B} = 400$ G, the ion temperature at the center of the plasma ($r = 0$ cm) is $\sim$0.38 eV and gradually decreases to $\sim$0.26 eV at $r = 7$ cm. The ion temperature generally increases with increasing magnetic field and develops a strong radial dependence. For the $\mathbf{B} = 600$ G, the ion temperature on axis is peaked at $\sim$0.51 eV and decreases smoothly to $\sim$0.3 eV at $r = 7$ cm. Thus, we see that as $\mathbf{B}$ is raised, the ion temperature at the center increases more than that at the edge of the plasma. As $\mathbf{B}$ is raised to 800 G, the ion temperature at the center increases further to being $\sim$0.56 eV $r = 0$, while at the edge ($r = 7$ cm), it is still $\sim$0.3 eV. The rate of increase of the central ion temperature seems to slow at higher magnetic fields as seen for $\mathbf{B} = 1000$ G ($T_{ion} \sim 0.58$ eV at $r = 0$ cm, and $\sim$0.35 eV at $r = 7$ cm). In Fig. 5(b), we show radial profiles for $\mathbf{B} = 1100$ G to $\mathbf{B} = 1400$ G. As noted earlier, at these conditions, the plasma is very turbulent with large intensity fluctuations in the density (strongest near the density gradient region of $3 < r < 5$ cm) and the electric fields. Moreover, the plasma density decreases by approximately an order of magnitude for $r \geq 6$ cm with respect to the center. Hence, the LIF signal in the edge region dropped, and we could not get reliable data even with integration for times up to 3 h (for the full 14 GHz). As a result, for these higher magnetic fields corresponding to turbulent plasmas, the data are reliable only out to $r = 6$ cm. For $\mathbf{B} = 1100$ G and 1200 G, the profiles are similar within experimental errors. The ion temperature at $r = 0$ cm is $\sim$0.64 eV, and it drops to $\sim$0.3 eV at $r = 6$ cm. For $\mathbf{B} = 1300$ G, there is a slight increase in the central peak of the ion temperature, $\sim$0.7 eV. We find that the increase in the ion temperature is noticeable only in the central region for $r < 2$ cm. For all $r > 3$ cm, the profiles are similar within experimental errors. For $\mathbf{B} = 1400$ G, we observe a marked increase in the central ion temperature ($\sim$0.81 eV), even though the edge temperature remains roughly the same, within the experimental errors. In addition to the strong ion heating at the center, as we increase the magnetic field to reach the global transition at 1400 G, the ion temperature gradient also increases, mostly for the central region around $r \sim 3$ cm.

In a similar way, Figs. 6(a) and 6(b) show the radial profiles of the azimuthal ion fluid velocity in the upgraded CSDX as the magnetic field is increased from 400 G to 1000 G, during the transition to drift wave turbulence, and

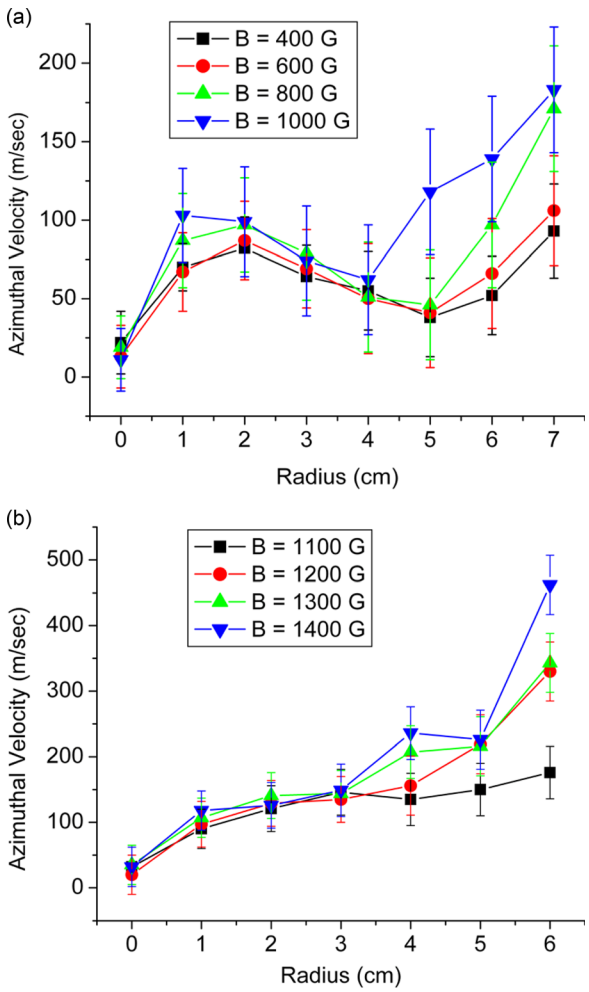

FIG. 6. (a) Radial profiles of the azimuthal ion fluid velocity for 400 G (black squares), 600 G (red circles), 800 G (green upright triangles), and 1000 G (blue inverted triangles). Positive velocity corresponds to flow in the electron diamagnetic drift direction. (b) Radial profiles of the azimuthal ion fluid velocity shown for 1100 G (black squares), 1200 G (red circles), 1300 G (green upright triangles), and 1400 G (blue inverted triangles). Positive velocity corresponds to flow in the electron diamagnetic drift direction.

separately from 1100 G to 1400 G, leading to the global transition, respectively. In these measurements, because the plasma density[7] decreased substantially beyond $r = 3$ cm, the errors in the measurements increase for larger radii. Moreover, as the turbulence levels increase, the scatter in the plots goes up significantly, even with multiple averaging, and hence we have larger errors in the measured velocity. Typical errors from the standard deviation of multiple measurements of the azimuthal velocity measurements for $r < 3$ cm are about ± 30 m/s and for $r > 4$ cm are approximately ± 50 m/s. As shown in Fig. 6(a), near the center of the plasma (for $r < 2$), the flow approximates solid body rotation (the azimuthal velocity increases almost linearly with distance). For relatively low magnetic fields, the maximum velocities reach about $\sim 90 \pm 20$ m/s at $r \sim 2$ cm and then slow down in the region $3 < r < 5$ cm. At larger radii of $r > 5$ cm, the azimuthal velocity again starts increasing. These radial variations in the azimuthal velocity profiles indicate deviation from a pure solid body rotation and confirm the presence of radially sheared azimuthal flow. The time averaged flows increase in general for the larger magnetic fields, and the corresponding shearing rate also goes up. For $\mathbf{B} = 1100$ G to $\mathbf{B} = 1400$ G, shown in Fig. 6(b), the general trend remains similar. In the inner core of the plasma, there is a solid body like rotation. Outside the core region, the rate of increase of the azimuthal velocity with radii saturates and the velocity plateaus in the region $2 < r < 4$ cm. There is a sharper increase in the azimuthal velocity at larger radii. The azimuthal ion fluid velocities at these increased magnetic fields thus exhibit strong flow shear in the edge region for $r > 4$ cm. The strength of the velocity shear increases with magnetic field as the system becomes more turbulent and approaches the global transition.

IV. DISCUSSION

The two main plasma parameters measured in these experiments, namely, the ion temperature and the azimuthal ion fluid velocity, help in understanding some of the observed features during the global transition that are detailed in Refs. 7 and 20. Here, we briefly summarize those results and explain the features that relate to the current study. For low to intermediate magnetic fields (400 G–1300 G), turbulence features systematically increase both in terms of being broader in the frequency spectra and in the intensity of fluctuations (see Fig. 8 of Ref. 7). Also, as the magnetic field increases, the central peak plasma density slowly increases at first and then saturates until at the transition it goes through another sudden $\sim 20\%$ increase (see Fig. 2(a) in Ref. 7). Below the magnetic field threshold for the transition ($\mathbf{B_{th}}$), the plasma rotates azimuthally only in the electron diamagnetic drift direction, being dominated by resistive drift waves with relatively low azimuthal mode numbers ($m \sim 1$–5). However, for $\mathbf{B} > \mathbf{B_{th}}$ we find a coherent mode with a high azimuthal mode number ($m \sim 10$–20) that propagates in the ion diamagnetic drift direction and is only limited to the core region of the plasma ($r < 2$ cm). We find evidence of this from high speed (210 500 frames per second) camera measurements as seen in Figs. 10 and 12 of Ref. 7. We also see this unambiguously from the conditional spectra of the light intensity fluctuations as shown in Fig. 10 of Ref. 20. Further, azimuthal plasma velocities inferred from time delay estimation also show this pattern of counter rotating plasma fluctuations for $\mathbf{B} > \mathbf{B_{th}}$.[7,18,20] For magnetic fields slightly lower than $\mathbf{B_{th}}$, we find that high m number waves do exist in the plasma, but intermittently and only at certain azimuthal locations of the plasma cross section.[19] Beyond the core, in the density gradient region ($3 < r < 5$ cm), resistive drift waves dominate. At even larger radii, near the edge plasma region ($r > 5$ cm), experimental signature point to strong shear driven instabilities based on the observations from fast imaging and probe measurements (from the relative strengths of the potential and density fluctuations and the phases differences between them as shown in Fig. 13 of Ref. 7). Both the resistive drift waves and the strong shear driven instabilities propagate in the electron diamagnetic drift direction.

In Fig. 7, we compare the changes in the radial profiles of the perpendicular ion temperature across the range of the magnetic field scan up to the transition (400 G–1400 G). In Fig. 8, we plot the radial profiles of the absolute values of the corresponding ion temperature gradients. We clearly see strong ion heating near the center of the plasma leading to the development of very strong ion temperature gradients at higher magnetic fields. For very low magnetic fields, the ion temperature is relatively flat and hence without significant gradients. As **B** is increased, we observe that the ion temperature gradient grows in magnitude and the peak in the gradient profile moves inwards. This seems to track the plasma density gradient in CSDX.[7] As the magnetic field is increased through low **B** up to the transition, the plasma density gradually increases and the plasma density gradient moves slightly inwards, possibly in response to an inward pinching effect[18,20] due to the confining effects of larger **B**. For the same range of **B**, using fast imaging, we find the appearance of a weak incomplete ion mode (high m modes, propagating in the ion diamagnetic drift direction) visible only near the high density peak of an $m = 1$ drift wave mode, even before the transition at $\mathbf{B_{th}}$. As we approach the transition, this ion mode gains in intensity and at the transition dominates the core region across the whole azimuthal range

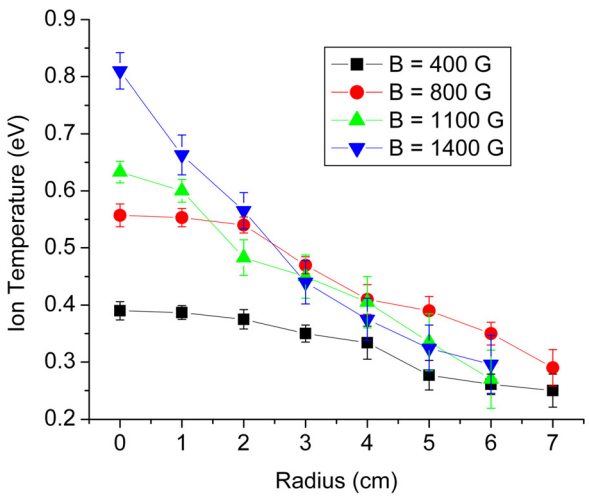

FIG. 7. Radial profiles of the perpendicular ion temperature shown for 400 G (black squares), 800 G (red circles), 1100 G (green upright triangles), and 1400 G (blue inverted triangles).

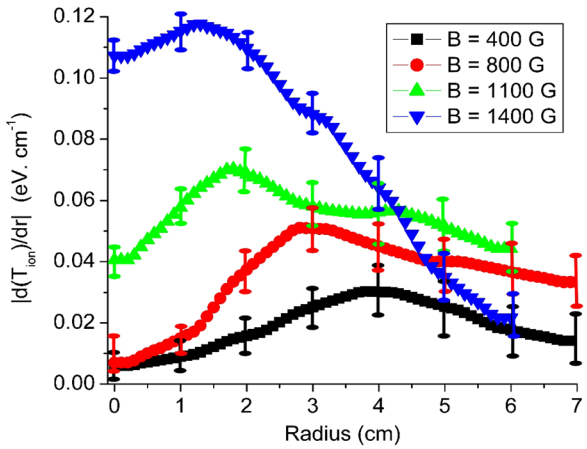

FIG. 8. Radial profiles of the absolute values of the perpendicular ion temperature gradients shown for 400 G (black squares), 800 G (red circles), 1100 G (green upright triangles), and 1400 G (blue inverted triangles). The gradient is calculated from the data in Fig. 6, interpolated on a grid of 1 mm radius, and then smoothed by averaging over 3 mm before taking the derivatives.

(and not just near the peak of the density maxima of the drift wave). At the transition, the core plasma density undergoes an increase of about 15%–20%, depending on source parameters. The ion mode tracks the density peak of the drift waves and is dominant only when the core density jumps at the transition. Hence, we hypothesize that the slightly higher plasma densities lead to increased electron-ion collisions (which are directly proportional to the plasma density) that effectively result in an increase of the ion temperatures. Consistent with this hypothesis, we find that the increase in the ion temperature is only near the center, where the increase in the plasma density is noticeable. At radii larger than 2–3 cm, there is no detectable change in either the plasma density or the ion temperature. Note that the ion temperature is still much smaller than the corresponding electron temperatures in CSDX for similar plasma parameters.[7] As the magnetic field approaches the global transition, the increased ion temperature gradient coincides with the appearance of strong coherent oscillations rotating in the ion diamagnetic drift direction.[7,20] This coherent mode appears only near the center, has very high azimuthal mode number ($m \sim 10$–20), and is also associated with enhanced Ar II emission from the plasma.[19] Thus, we find that an ion feature is formed which rotates in the ion diamagnetic drift direction, is localized to the region in space when the ion temperature gradient is significant, is coincident with the observation of a higher ion temperature gradient, and leads to stronger ion emission. The characteristics of this ion mode seem to point to an ion temperature gradient driven instability. Linear stability analysis using the experimentally measured radial profiles is underway. This ion mode instability and the drift wave instability due to the density gradient coexist. For $\mathbf{B} < \mathbf{B_{th}}$, we find that the drift waves modes are dominant, as they carry the ion mode fluctuations in the electron diamagnetic drift direction with them. But for $\mathbf{B} > \mathbf{B_{th}}$, the ion mode at the center gains enough energy to dominate over the drift waves in the core plasma region and we observe stable, coherent, high azimuthal mode number fluctuations rotating in the ion diamagnetic drift direction[7,19,20] at $\mathbf{B} = 1400$ G.

From the profiles in Fig. 8, we see that the most significant gradient in the ion temperature is observed at 1400 G, just after the global transition. To obtain this plot, we have interpolated the experimentally measured ion temperature values shown in Fig. 7 on to a grid of 1 mm radius and used a sliding average algorithm to smoothen the radial profile of ion temperature by averaging over a distance of 3 mm. We then took the radial derivative and again smoothed the resulting derivative by averaging over a radii 3 mm. Note that not only the intensity of the ion temperature gradient increases with increasing magnetic field but also the peak of the ion temperature gradient also moves inward in radii at higher **B**. At ~1300 G, we see the formation of the helicon blue core, which leads to a tenfold increase in the central Ar II light intensity, simultaneously along with the global transition.[7,19] Using passive optical emission spectroscopy, we also find that the ion mode is associated with stronger Ar II emission with the appearance of many new lines in the emission spectra. Detailed spectroscopy of the transition to the helicon core mode is being performed and will be shown in a later publication. The increased ion heating in the core region (presumably due to increased electron ion collisions at slightly higher density) gives rise to the ion mode. When this ion mode becomes stronger than the drift modes, the transition occurs. Such a local change of the dominant turbulence mode is similar to the transition from Linear Ohmic Confinement (LOC) mode to Saturated Ohmic Confinement (SOC) mode in tokamaks.[11,12] However, as **B** is raised well beyond $\mathbf{B_{th}}$, the coherence of the core ion mode in CSDX seems to go down, as shown by the increased noise in the radial profiles of the density and potential spectra (shown in Fig. 8 of Ref. 7). Simultaneously, we see relaxation of all the plasma gradients, such as the plasma density, electron temperature, and edge electric fields with further increase in the magnetic field. Fig. 9 shows the ion temperature at the center of the plasma over the whole range of this experiment (400 G–1800 G), and we see the maximum ion heating occurs right after the transition which occurs between 1300 G and 1400 G. Subsequently, the core ion temperature drops for magnetic fields beyond the transition. Since the edge ion temperatures remain similar, the ion temperature gradients also decrease for the larger magnetic fields. The relaxation of the plasma profiles seems correlated to observations that the edge of the plasma is very turbulent (which are driven by strongly sheared azimuthal flows), and the core ion mode is no longer very coherent for magnetic fields beyond the transition.

In Fig. 10, we compare the changes in the radial profiles of the azimuthal ion fluid velocities as measured by LIF across the whole range of the magnetic field up to the transition (400 G–1400 G). We can clearly see the development of strong flows at large radii and corresponding edge shear at higher magnetic fields. Even though we could not measure the velocities for large radii near the edge of the device due to the lack of enough plasma density and hence LIF signal, it is expected that high neutral densities provide large damping to azimuthal ion flows,[5,32] and hence, the velocity should

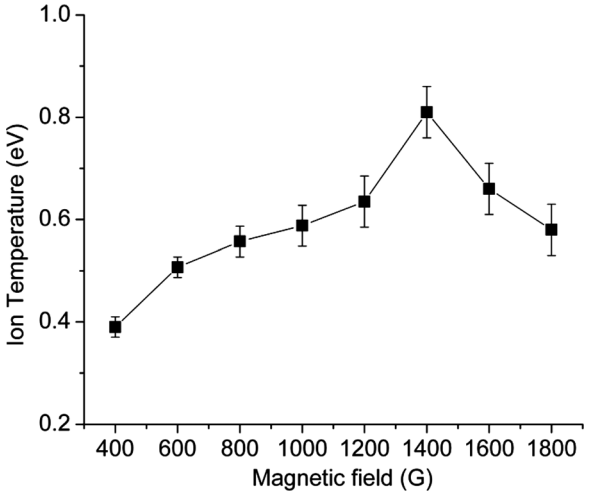

FIG. 9. Ion temperature measured at $r = 0$ cm as the magnetic field is changed. We observe a more pronounced increase in the core ion temperature going into the transition between 1300 G and 1400 G (and thus leading to strong ion temperature gradients near the center), after which the profile relaxes.

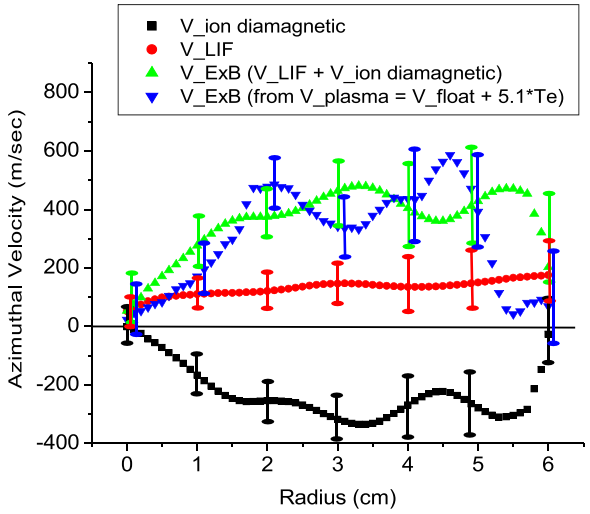

FIG. 11. Radial profiles of the various relevant azimuthal velocities in CSDX: ion diamagnetic drift velocity (black squares), ion fluid velocity as measured by LIF (red circles), and the net effective $\mathbf{E} \times \mathbf{B}$ velocity (green triangles), shown for $\mathbf{B} = 1100$ G. Positive velocity corresponds to flow in the electron diamagnetic drift direction. The typical errors in the calculated $\mathbf{E} \times \mathbf{B}$ velocities are about ± 60 m/s for $r < 3$ cm and ± 90 m/s for $r > 4$ cm.

decrease for the radii close to the chamber wall. LIF measurements give an absolute Doppler shifted velocity of the ions in the volume of interrogation and thus represent the bulk flow of the ions. Consistent measurements of flows in plasmas are nontrivial as there can be many contributions to the total plasma velocities involved; for example, the phase velocities of waves can be superimposed on top of the rotating background plasma that sustains the waves. In CSDX, the fluid plasma flows observed with LIF are in the electron diamagnetic drift direction. The LIF measurements are effectively a vector sum of the $\mathbf{E} \times \mathbf{B}$ velocity (due to the radial potential gradients set up by the plasma) and the ion diamagnetic drift associated with the ion pressure gradients.

Using the measured radial profiles of ion temperature and density, the contribution of the ion diamagnetic drift to the net measured LIF ion fluid velocity is calculable. Thus, from the LIF measurements and the ion diamagnetic field

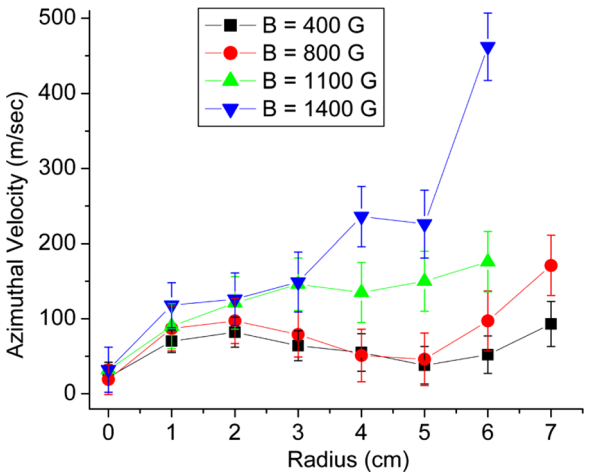

FIG. 10. Radial profiles of the azimuthal ion fluid velocity shown for 400 G (black squares), 800 G (red circles), 1100 G (green upright triangles), and 1400 G (blue inverted triangles). Positive velocity corresponds to flow in the electron diamagnetic drift direction.

contributions, the $\mathbf{E} \times \mathbf{B}$ velocity is calculable. In Fig. 11, we show the radial profiles of the $\mathbf{E} \times \mathbf{B}$ flow, calculated from the LIF velocity and the ion diamagnetic drift for a representative magnetic field (1100 G), and compare that to the $\mathbf{E} \times \mathbf{B}$ flow as measured from the estimated plasma potential (from a combination of the measured floating potential and the electron temperature). To calculate the ion diamagnetic drifts, we again interpolate the ion temperature and plasma density profiles to a grid of 1 mm, to take the necessary derivatives, and then smooth by radially averaging over 3 mm. In this approach, it is assumed that the bulk plasma flow as measured by LIF and the ion diamagnetic drift driven by the ion pressure gradient are the only two dominant mechanisms that contribute to the net $\mathbf{E} \times \mathbf{B}$ rotation, and all other effects, for example, the ion momentum gained due to neutral collisions, are neglected. In a similar way, we can calculate the $\mathbf{E} \times \mathbf{B}$ velocity for the other magnetic fields. In Fig. 12, we show the $\mathbf{E} \times \mathbf{B}$ velocities for the magnetic fields leading to the transition. We see that the effective $\mathbf{E} \times \mathbf{B}$ velocity before and after the transition is quite different. Before the transition (shown for $\mathbf{B} = 1000$ G and 1200 G), the $\mathbf{E} \times \mathbf{B}$ velocities are consistent with solid body rotation near the center for $r < 3$ cm and then saturate around maximum velocities of $\sim$400 m/s. However, after the transition (shown for $\mathbf{B} = 1300$ G and 1400 G), the $\mathbf{E} \times \mathbf{B}$ velocities at the large radii ($\sim r = 5$ cm) increase rapidly and reach a maximum peak of $\sim$700 m/s, producing strongly sheared flows. This strong shear in the $\mathbf{E} \times \mathbf{B}$ velocities at the transition is consistent with imaging data,[7] which is suggestive of Kelvin-Helmholtz like shear driven instabilities at the edge. We note that the ion sound speed in CSDX plasmas at these electron temperatures is $\sim$3 km/s, and hence, the azimuthal flows that we find are subsonic.

In conclusion, we see that as the plasma becomes more turbulent, at higher magnetic fields, the ion temperature

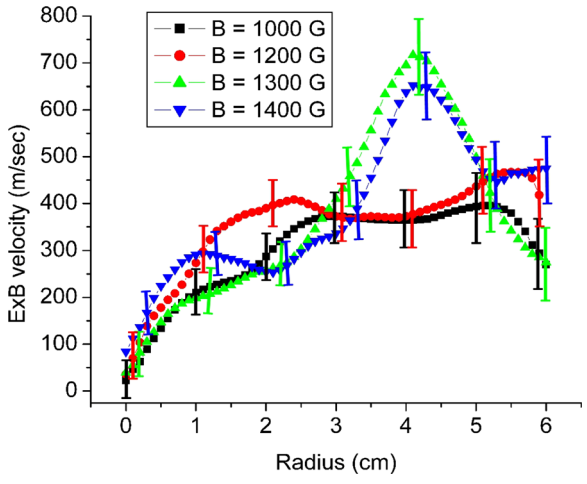

FIG. 12. Comparison of the radial profiles of the E × B drift velocity for the magnetic fields leading up to the transition: 1000 G (black squares), 1200 G (red circles), 1300 G (green upright triangles), and 1400 G (blue inverted triangles). The typical errors in the calculated **E** × **B** velocities are about ±60 m/s for $r < 3$ cm and ±90 m/s for $r > 4$ cm. Positive velocity corresponds to flow in the electron diamagnetic drift direction.

profile steepens and simultaneously the velocity shear at the edge increases in magnitude. The steepening of the ion temperature profiles can possibly drive an ion temperature gradient driven instability, which competes with the existing drift instability driven by the background plasma density gradient. The sheared **E** × **B** flow is also found to grow stronger with increasing magnetic field. Beyond a certain threshold, the ion temperature gradient increases markedly and a dominant coherent ion mode develops in the core, a global transition in the plasma. Simultaneously, we find dramatic changes in the radial particle flux and observe locally inward, up gradient, particle flux that leads to the formation of a radial particle transport barrier. This global transition has strong hysteresis and is reminiscent of a standard transport bifurcation.[20] Simultaneously, the strongly sheared flows at the edge help in the formation of a radial particle transport barrier and stabilize the core, leading to the formation of steep pedestal-like gradients in the plasma density and the ion pressure profiles. The measurements of the ion temperature profiles and the ion fluid velocities are critical to understanding the details of the observations in Refs. 7 and 20.

In addition, the ion temperature measurements are needed to compute the ion-ion collisional viscosity profiles, required for studying the momentum balance between the Reynolds stress and the flow damping.[5,31] We are currently working on the details of the momentum balance by including these new ion temperature profiles on the upgraded CSDX, and those results will be published later. The only other experimentally relevant parameter for turbulent momentum balance that has not yet been measured in CSDX is the radial profile of the neutral gas density. Although calculations suggest that the effect of spatial variations in the neutral gas density is smaller than the effects of spatial variations in the ion temperature, it would be useful to obtain actual measurements of the neutral density profile. In future experiments, we intend to measure the radial profile of neutral gas density in CSDX with LIF.[33,34]

ACKNOWLEDGMENTS

The UCSD contributions to this work were supported by the Center for Momentum Transport and Flow Organization, DE-SC0008378, and the WVU contributions to this work were supported by NSF Award No. PHY-1360278.

[1]W. Horton, Rev. Mod. Phys. **71**, 735 (1999).
[2]G. R. Tynan, A. Fujisawa, and G. Mckee, Plasma Phys. Controlled Fusion **51**, 113001 (2009).
[3]P. H. Diamond, S.-I. Itoh, K. Itoh, and T. S. Hahm, Plasma Phys. Controlled Fusion **47**, R35 (2005).
[4]M. J. Burin, G. R. Tynan, G. Y. Antar, N. A. Crocker, and C. Holland, Phys. Plasmas **12**, 052320 (2005).
[5]G. R. Tynan, C. Holland, J. H. Yu, A. James, D. Nishijima, M. Shimada, and N. Taheri, Plasma Phys. Controlled Fusion **48**, S51 (2006).
[6]P. Manz, M. Xu, S. C. Thakur, and G. R. Tynan, Plasma Phys. Controlled Fusion **53**, 095001 (2011).
[7]S. C. Thakur, C. Brandt, L. Cui, J. J. Gosselin, A. D. Light, and G. R. Tynan, Plasma Sources Sci. Technol. **23**, 044006 (2014).
[8]Y. Nagashima, S. I. Itoh, S. Shinohara, M. Fukao, A. Fujisawa, K. Terasaka, Y. Kawai, G. R. Tynan, P. H. Diamond, M. Yagi, S. Inagaki, T. Yamada, and K. Itoh, Phys. Plasmas **16**, 020706 (2009).
[9]T. Windisch, O. Grulke, and T. Klinger, J. Nucl. Mater. **390**, 395 (2009).
[10]T. A. Carter and J. E. Maggs, Phys. Plasmas **16**, 012304 (2009).
[11]C. L. Rettig, T. L. Rhodes, J. N. Leboeuf, W. A. Peebles, E. J. Doyle, G. M. Staebler, K. H. Burrellr, and R. A. Moyer, Phys. Plasmas **8**, 2232 (2001).
[12]J. E. Rice, M. J. Greenwald, Y. A. Podpaly, M. L. Reinke, P. H. Diamond, J. W. Hughes, N. T. Howard, Y. Ma, I. Cziegler, B. P. Duval *et al.*, Phys Plasmas **19**, 056106 (2012).
[13]E. Thomas, Jr., J. D. Jackson, E. A. Wallace, and G. Ganguli, Phys. Plasmas **10**, 1191 (2003).
[14]S. C. Thakur, M. Xu, P. Manz, N. Fedorczak, C. Holland, and G. R. Tynan, Phys. Plasmas **20**, 012304 (2013).
[15]D. A. D'Ippolito, D. A. Russell, J. R. Myra, S. C. Thakur, G. R. Tynan, and C. Holland, Phys. Plasmas **19**, 102301 (2012).
[16]M. Xu, G. R. Tynan, C. Holland, Z. Yan, S. H. Muller, and J. H. Yu, Phys. Plasmas **17**, 032311 (2010).
[17]A. D. Light, S. C. Thakur, C. Brandt, Y. Sechrest, G. R. Tynan, and T. Munsat, Phys. Plasmas **20**, 082120 (2013).
[18]L. Cui, G. R. Tynan, P. H. Diamond, S. C. Thakur, and C. Brandt, Phys. Plasmas **22**, 050704 (2015).
[19]S. C. Thakur, C. Brandt, L. Cui, J. J. Gosselin, and G. R. Tynan, IEEE Trans. Plasma Science **43**, 2754 (2015).
[20]L. Cui, A. Ashourvan, S. C. Thakur, R. Hong, P. H. Diamond, and G. R. Tynan, Phys. Plasmas **23**, 055704 (2016).
[21]R. W. Boswell, Plasma Phys. Controlled Fusion **26**, 1147 (1984).
[22]A. M. Keesee, R. Boivin, and E. E. Scime, Rev. Sci. Instrum. **75**, 4091 (2004).
[23]A. Aanesland, L. Liard, G. Leray, J. Jolly, and P. Chabert, Appl. Phys. Lett. **91**, 121502 (2007).
[24]G. Severn, L. Dongsoo, and N. Hershkowitz, Rev. Sci. Instrum. **78**, 116105 (2007).
[25]S. C. Thakur, C. Brandt, A. Light, L. Cui, J. J. Gosselin, and G. R. Tynan, Rev. Sci. Instrum. **85**, 11E813 (2014).
[26]S. C. Thakur, D. McCarren, T. Lee, N. Fedorczak, P. Manz, E. E. Scime, G. R. Tynan, and M. Xu, Phys. Plasmas **19**, 082102 (2012).
[27]S. C. Thakur, D. McCarren, T. Lee, N. Fedorczak, P. Manz, E. E. Scime, G. R. Tynan, M. Xu, and J. Yu, Rev. Sci. Instrum. **83**, 10D708 (2012).
[28]G. D. Severn, D. A. Edrich, and R. McWilliams, Rev. Sci. Instrum. **69**, 10 (1998).
[29]R. F. Boivin, *Zeeman Splitting for LIF Transitions and De-Convolution Technique to Extract Ion Temperatures, PL-050* (West Virginia University, Morgantown, USA, 2002).
[30]R. F. Boivin, *Study of the Different Line Broadening Mechanisms for the Laser Induced Fluorescence Diagnostic of the HELIX and LEIA Plasmas, PL-039* (West Virginia University, Morgantown, USA, 2002).
[31]J. J. Gosselin, S. C. Thakur, S. H. Sears, J. S. McKee, E. E. Scime, and G. R. Tynan, Phys. Plasmas **23**, 073519 (2016).
[32]C. Holland, J. H. Yu, A. James, D. Nishijima, M. Shimada, N. Taheri, and G. R. Tynan, Phys. Rev. Lett. **96**, 195002 (2006).
[33]A. Keesee and E. E. Scime, Rev. Sci. Instrum. **77**, 10F304 (2006).
[34]A. Keesee and E. E. Scime, Plasma Sources Sci. Technol. **16**, 742 (2007).